Geometrical evaluation on the viscous effect of point-absorber wave-energy converters

CHEN Zhong-fei[a], ZHOU Bin-zhen[a,*], ZHANG Liang[a,*], ZHANG Wan-chao[b], WANG Shu-qi[b], ZANG Jun[c]

[a]*College of Shipbuilding Engineering, Harbin Engineering University, Harbin 150001, China*
[b]*School of naval structure and ocean engineering, Jiangsu University of Science and Technology, Zhenjiang 212003, China*
[c]*Department of Civil and Architecture Engineering, University of Bath, Bath, BA2 7AY, UK*

ABSTRACT

The fluid viscosity is known to have a significant effect on the hydrodynamic characteristics which are linked to the power conversion ability of wave energy converter (WEC). To overcome the disadvantages of case-by-case study through the experiments and numerical computation employed by the former researches, the viscous effect is studied comprehensively for multiple geometries in the present paper. The viscous effect is expressed as viscous added mass and damping solved by the free-decay method. The computational fluid dynamics (CFD) method is employed for the calculation of the motion and flow field around the floater. The diameter to draft ratio and bottom shape are considered for the geometrical evaluation on the viscous effect. The results show that a slenderer floater presents a stronger viscous effect. Through the comparisons of the floaters with four different bottom shapes, the conical bottom is recommended in terms of low viscous effect and simple geometry for manufacture. A viscous correction formula for a series of cylindrical floaters is put forward, for the first time, to help the engineering design of outer-floaters of point-absorber WECs.

Key words: Viscous effect; Wave energy convertor; Multiple geometries; Viscous correction; CFD

1. Introduction

Wave energy convertors (WECs) can be divided into three categories according to the relative position between the predominant wave direction and WECs, namely attenuator, terminator, and point absorber (PA-WEC) (Drew et al., 2009). A PA-WEC possesses small dimension relative to the incident wavelength, so that it is easy for array arrangement. Mccabe et al. (2009) argued that the PA-WEC is the most efficient in terms of wave-power conversion per unit volume. This feature makes it highly suitable for the seas with

Foundation item: This work was financially supported by the National Natural Science Foundation of China (Grant Nos. 51761135013), the High Technology Ship Scientific Research Project from Ministry of Industry and Information Technology of the People's Republic of China–Floating Security Platform Project (the second stage, 201622), and the Fundamental Research Fund for the Central University (HEUCF180104, HEUCFP201809), the China Scholarship Council (the International Clean Energy Talent Programme, 2017).

*Corresponding author. E-mail: zhoubinzhen@hrbeu.edu.cn (B.Z. Zhou), zhangliang@hrbeu.edu.cn (L. Zhang).

relatively low wave energy density, e. g., Chinese adjacent seas (Wu et al., 2015). In these areas, the wave energy may not be able to produce enough electricity steadily for main-land grids, while it could be an effective supplement for the net-off microgrids of islands, oil platforms, or other offshore marine structures (Babarit et al., 2006).

For PA-WECs that work in heave mode, axial-symmetrical floaters are normally adopted to reduce the sensibility of wave directions, such as the CETO (Australia) (Penesis et al., 2016), PowerBuoy (USA) (Edwards and Mekhiche, 2014), Wavebob (Ireland) (Weber et al., 2009), etc. The hydrodynamic characteristic of PA-WECs is needed to be studied in detail to maximize the wave power absorption. Generally, there are mainly three types of methods for solving hydrodynamic properties of PA-WECs: Analytical method, Boundary Element Method (BEM), and computational fluid dynamics (CFD). A comprehensive review can be found in Li et al. (2012). The linear potential flow theory could highly overestimate the motion and power response of a PA-WEC (Jin & Patton., 2017) because of ignoring the viscous effect. Especially when it is around the resonance frequency, the response simulated by non-viscous linear potential flow theory could be more than 10 times larger than that of the experiment, see examples in Tom (2013). The viscous effect can inevitably reduce the ability of wave power conversion of a PA-WEC, as shown in Son et al. (2016), Li & Yu (2012), and Tom (2013).

The viscous effect of PA-WECs was studied experimentally or numerically by many researchers. Through the experimental study, Vantorre et al. (2004) argued that, a floater with rounded-edge bottom has less energy dissipation due to viscosity. Yeung & Jiang (2011) explored the viscous damping and added mass of four two-dimensional heaving floaters by a viscous method called the Free-Surface Random-Vortex Method (FSRVM). Jin & Patton (2017) studied three cylindrical floaters by the viscous CFD software LS-DYNA and the results demonstrated that the rounded- and conical-bottom floaters had less viscous damping than that with the flat-bottom. Palm et al. (2016) investigated a PA-WEC with a slack-moored cylinder through the OpenFOAM with the consideration of viscosity and green-water effect. Bhinder et al. (2011) and Caska et al. (2008) studied PA-WECs with generic cylindrical floaters working in heave and pitch modes, respectively, by introducing a Morison-like non-linear quadratic damping term. There are also many studies on other types of WECs that considered the fluid viscosity, such as the OWC (oscillating water column) (Ning et al., 2015 and 2016), a flap-type terminator (Chen et al., 2015), and a Rolling WEC (Jiang, 2015), etc.

In the published literatures, most studies on the effect of fluid viscosity were specific for a few given floaters. Even when different bottom shapes (such as Jin & Patton, 2017 and Yeung & Jiang, 2012) were considered, no detailed slenderness parameter studies have been provided. In our study, we consider not only different bottom shapes, but also the slenderness. The viscous effect is expressed by the linearized viscous damping and added mass corrections. The viscous hydrodynamic quantities are acquired by free-decay curves calculated by Reynolds-Averaged Navier-Stokes (RANS) and Volume of Fluid (VOF)

method based on a CFD commercial software StarCCM+. And then the viscous corrections can be obtained by comparing the viscous and potential radiation forces. Most importantly, through the curve fitting technology, a correction formula is derived for both viscous damping and added mass for the first time. This formula can be directly applied to the performance evaluation and the geometrical design of the absorber with fast speed. An example application of the viscous correction formula to the floater geometry design is demonstrated.

2. Methodology

The viscous effect of the floater of a PA-WEC considering only heave mode is simplified and expressed in this section. The numerical and experimental studies conducted by Tom (2013) and Son et al. (2016) demonstrated that the excitation forces could be well predicted by the linear potential flow theory, while the radiation forces (especially the damping term) are significantly affected by the viscous effect. Therefore, the viscous effect should be studied mainly on the radiation force

The radiation force is the hydrodynamic force acting on the floating body by the radiation wave field generated by the body motion, which can be expressed as

$$F_r = -\mu_{33}\ddot{} \qquad \dot{} \tag{1}$$

where μ_{33}, λ_{33} are the potential added mass and radiation damping which are calculated by AQWA in frequency domain based on the Boundary Element Method (BEM). The velocity and acceleration of the body are denoted by $\dot{}$ and $\ddot{}$, respectively. Similarly, the radiation force considering the viscosity can be expressed as

$$F_{r,vis} = -\mu_{vis}\ddot{} \qquad \dot{} \tag{2}$$

where μ_{vis} and λ_{vis} denote the linearized added mass and damping in the viscous fluid, respectively.

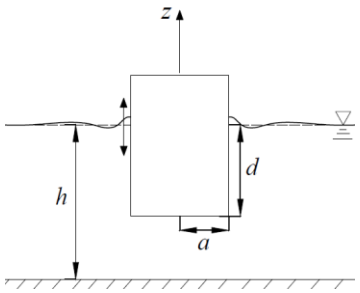

Fig.1. Schematic of cylindrical floater in heave free-decay motion

As shown in Fig.1, the radius of the floater is a and the draft is d. The water depth is h. The motion equation of a floater in heave free-decay motion can be written as

$$(M+\mu_{vis})\ddot{x}_3+\dot{x}_3+C_3x_3=0 \tag{3}$$

where M is the mass of the floater, x_3 is the heave motion of the floater, C_3 is the hydrostatic restoring force coefficient. For cylindrical floaters, $C_3=\rho g\pi a^2$ with water density ρ and gravity acceleration g. By setting the initial velocity as zero and the initial excursion as x_{30}, the displacement can be obtained by

$$x_3=x_{3,a}e^{-\nu t}\cos\left(\omega_{3,vis}t-\varphi_3\right) \tag{4}$$

where $x_{3,a}=x_{30}\sqrt{1+\left(\nu/\omega_{3,vis}\right)^2}$. $\omega_{3,vis}=\sqrt{\omega_3^2-\nu^2}$ is the damped resonance frequency, $\omega_3=\sqrt{C_3/(M+\mu_{vis})}$ is the undamped resonance frequency, $\nu=\lambda_{vis}/(M+\mu_{vis})$ is the decay factor, $\varphi_3=\tan^{-1}(\nu/\omega_{3,vis})$ is the phase angle. For a larger x_{30}, the equivalent viscous damping is larger (Tom, 2013). The experimental study of Tom (2013) proved that, when setting $x_{30}\approx 0.35\sim 0.4d$, the viscous hydrodynamic coefficients from free-decay tests matched very well with that from the regular-wave experiments. For engineering applications, the prediction of the performance of a PA-WEC in waves should be conservative and therefore a relatively large value of x_{30} is chosen, i.e., $x_{30}=0.4d$.

The decay factor ν can be derived by the logarithmic decrements of the peaks of a free-decay curve (e.g. Tom, 2013)

$$\nu=\frac{2}{T_{3,vis}}\cdot\frac{1}{N-1}\sum_{k=1}^{N-1}\ln\frac{x_{3,k}}{x_{3,k+1}} \tag{5}$$

where $T_{3,vis}=2\pi/\omega_{3,vis}$ is the damped resonance period, $x_{3,k}$ is the amplitude of the k-th peak of a free-decay curve, N is the number of peaks. Accordingly, the added mass and damping in the viscous fluid can be calculated by

$$\mu_{vis}=\frac{C_3}{\omega_{3,vis}^2+\nu^2}-M,\ \lambda_{vis}=2\nu\left(M+\mu_{vis}\right) \tag{6}$$

The non-dimensional linearized viscous corrections are defined as

$$\bar{f}_{\mu,vis}=\mu_{vis}/\mu_{33},\ \bar{f}_{\lambda,vis}=\lambda_{vis}/\lambda_{33} \tag{7}$$

The physical meaning of $\bar{f}_{\mu,vis}$ and $\bar{f}_{\lambda,vis}$ shows the ratio of the viscous added mass or damping and the potential added mass or damping. Similar notation method can be found in Son et al. (2016), Tom (2013), and Wang et al. (2016), etc.

Consequently, the radiation force in viscous flow fluid Eq.(2) can be expressed in the form of

$$F_{r,vis}=-\bar{f}_{\mu,vis}\mu_{33}\ddot{x}_3-\bar{f}_{\lambda,vis}\lambda_{33}\dot{x}_3 \tag{8}$$

The CFD software Star CCM+ is used to simulate the free-decay motion of the cylindrical floater in heave mode. The free surface is tracked by the VOF method and the Dynamic Fluid/Body Interaction (DFBI) module with the overset mesh adopted to simulate the motion of the body.

The numerical wave tank (NWT) is shown in 0. Most of the regions are hexahedron structural meshes, only around the corner or the bottom with complex geometry are tetrahedron non-structural meshes. To avoid the non-structural mesh at rounded boundaries, a rectangular NWT is adopted instead of a cylindrical one. The length and width of the numerical domain are equal because there is no need of incident wave generation. To avoid wave reflection from the NWT boundary, the length and width are set more than 20 times of the radius of the cylinder and 1/3 of the NWT from both wall boundaries are damping zone for absorbing radiation waves.

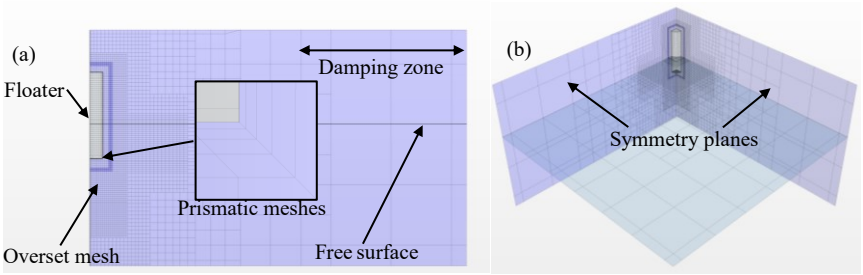

Fig.2. Sectional (a) and axonometric (b) view of the mesh grid of the numerical wave tank, and a flat-bottom cylindrical floater with $2a/d$=0.3 is shown as an example.

Four layers of prismatic meshes are used near the surface of the floater to increase the simulation quality of the boundary layer (Fig.2 (a)). For the balance of the simulation efficiency and accuracy, the mesh size grows larger as the distance to the floater increases as demonstrated in 0. The finer meshes are used around the floater and the free surface. Through convergence tests of space and time as shown in Fig.3, the minimum mesh length is taken as $d/30$, and the time step is $T_{res}/200$, where T_{res} is the non-damped resonance period and can be calculated by the linear potential theory. For the example shown in Fig.3 ($d/30$ & $T_{res}/200$), the number of the total cells is 84,767 and the total CPU time is 1.8h with a quad-core Intel Core i7-6700 CPU (3.40GHz, 64-bit).

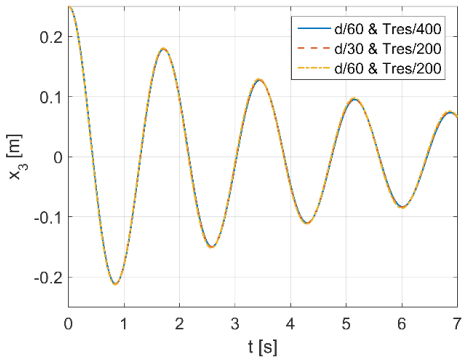

Fig.3. Convergence study for different, minimum mesh sizes, and time steps with $2a/d$=0.3, x_{30}=0.4d.

To verify the accuracy of the present numerical method, we compare the numerical results with data from the experiment of Tom (2013) for two cylindrical floaters with different bottom shapes. One is with the flat bottom ($2a$=0.273m and d=0.613m) and the other is with the rounded bottom ($2a$=0.273m and d=0.706m). The draft of the rounded bottom in the literature (Tom, 2013) means the distance from the mean water plane to the lowest point of the rounded bottom. As illustrated in Fig.4, the free-decay curves matched very well between the experimental data and the present numerical results. The largest differences are around the peaks, while other areas are matched perfectly. The mean difference of the amplitudes is less than 4.0%. Therefore, the numerical method is confirmed to be capable of simulating the free-decay motion with high accuracy.

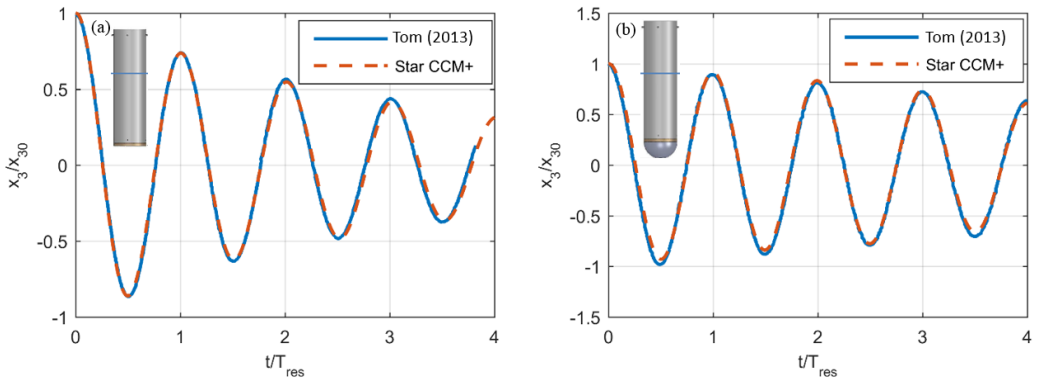

Fig.4. Comparison of free-decay curves with the experiment data (Tom, 2013)[1], (a) Flat bottom, (b) Rounded bottom.

3. Geometrical evaluation on viscous effect

3.1. Diameter to draft ratio

The floaters considered in this paper are axial-symmetric, so that the characteristic of the geometry can be denoted by only one variable, i.e., the diameter to draft ratio $2a/d$. The floater becomes fatter as $2a/d$ increases. Fig.5 shows that the viscous effect (both added mass and damping) are greatly influenced by $2a/d$. As $2a/d$ increases, $\bar{f}_{\mu,vis}$ and $\bar{f}_{\lambda,vis}$ both decrease. This reveals that a fatter floater has less viscous effect. $\bar{f}_{\mu,vis}$ and $\bar{f}_{\lambda,vis}$ are both asymptotic to 1.0 when $2a/d$ increases. This means that the viscous effect of a very fat floater is inappreciable.

[1] The experiment data in Tom, (2013) is open access. The link is http://digitalassets.lib.berkeley.edu/etd/ucb/text/Tom_berkeley_0028E_14051.pdf (last access: May 7, 2018)

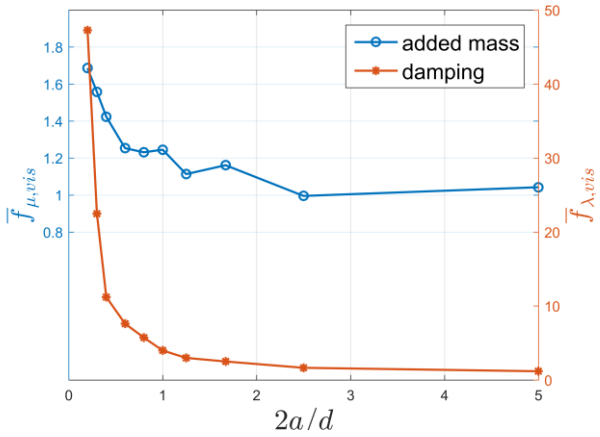

Fig.5. Viscous corrections of flat bottom cylindrical floaters with different $2a/d$.

The damping of a floater in the viscous fluid λ_{vis} comes from two parts: One is potential radiation damping and the other is viscous dissipation, which mainly consists of viscous friction and vortex shedding (Bhinder et al., 2011). The expression of the viscous effect in the present paper is the ratio of the total damping in viscous fluid to the damping in potential fluid, $\overline{f}_{\lambda,vis} = \lambda_{vis} / \lambda_{33}$. By the nondimensionalization of damping as $\overline{\lambda}_{vis\ or\ 33} = \lambda_{vis\ or\ 33} / \pi\rho a^2 \sqrt{gd}$, the viscous damping correction coefficient can also be in the form of $\overline{f}_{\lambda,vis} = \overline{\lambda}_{vis} / \overline{\lambda}_{33}$. The comparison between $\overline{\lambda}_{vis}$ and $\overline{\lambda}_{33}$ is shown in Fig.6. It reveals that $\overline{\lambda}_{vis}$ and $\overline{\lambda}_{33}$ both increase with $2a/d$ increasing. The difference of $\overline{\lambda}_{vis}$ and $\overline{\lambda}_{33}$ denotes the contribution of viscous dissipation. Fig.6 illustrates that the increments of $\overline{\lambda}_{vis} - \overline{\lambda}_{33}$ is relatively small compared with that of $\overline{\lambda}_{33}$ which is the denominator of $\overline{f}_{\lambda,vis} = \overline{\lambda}_{vis} / \overline{\lambda}_{33}$. This means that $\overline{\lambda}_{vis} \approx \overline{\lambda}_{33}$ for a fat floater. That is, the viscous effect for a fat cylindrical floater can be neglected.

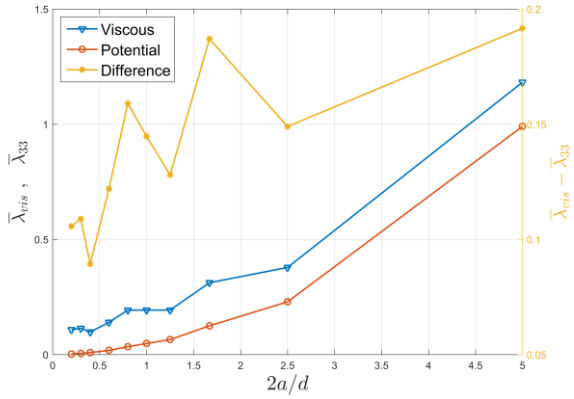

Fig.6. Viscous damping and potential damping of flat bottom cylindrical floaters with different $2a/d$.

3.2. Bottom shape

This section studies the influence of bottom shape on the viscous effect. As illustrated in Fig.7 (a) to (d), four different bottom shapes are considered, they are: flat bottom (FB), rounded bottom (RB), conical

bottom (CB) and Berkeley Wedge bottom (BWB). Practically, the needlelike tip of the BWB brings extra difficulty in manufacturing and may have structure strength problem. Therefore, the needlelike tip should be substituted by a small hemisphere (e.g. with the radius 0.1a), as shown in Fig.7(e) and named BWB-H (H stands for the small hemisphere). For the CB, the taper angle coefficient is defined as TAC=h_{cone}/a, where h_{cone} is the height of the cone. Firstly, TAC=3.0 is taken as an example, and the effect of TAC on the viscous effect is discussed in the following. The Berkeley Wedge (BW) is a two-dimensional needlelike curve developed by Madhi et al. (2014) and meant to diminish the viscous damping in heave mode. In this paper, we pivot the two-dimensional BW curve to form a three-dimensional cylindrical floater with a BWB.

For a non-FB floater, the submerged part under the mean water line consists of two parts, one is vertical cylindrical parts with height of d_{cylin} and the other is the non-flat bottom part with volume of V_{bottom}. To study the effect of the bottom shape, the displacements (or masses) are taken the same for floaters with different bottom shapes. Therefore, d_{cylin} of different non-FB floaters can be calculated as

$$d_{cylin} = \frac{V - V_{bottom}}{\pi a^2} \tag{9}$$

where V and a are the displacement and the radius of the floater, respectively. For example, for floaters with $2a/d$=1.0 (Fig.7), d_{cylin} are 0.50d, 0.67d, and 0.57d for the CB, RB, BWB floaters, respectively. Moreover, for the convenience in the discussion of the parameter $2a/d$ for non-FB floaters, the concept of equivalent draft d is defined, which is the same as the FB floater, see examples in Fig.7.

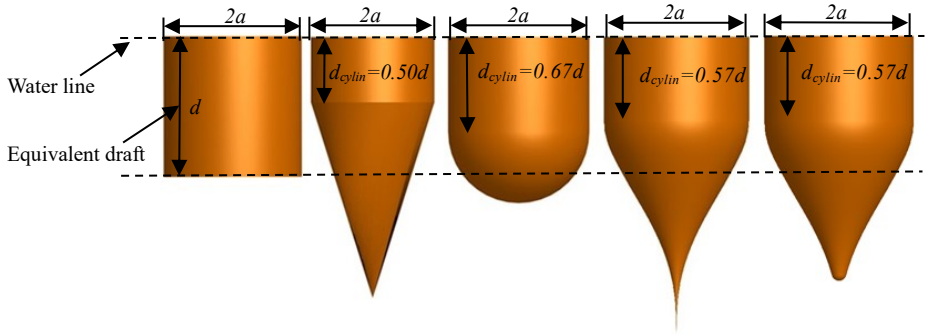

(a) FB (b) CB (c) RB (d) BWB (e) BWB-H

Fig.7. The submerged part of cylindrical floaters with different bottom shapes, with $2a/d$=1.0 as an example.

The free-decay curves for these floaters are illustrated in Fig.8 and the corresponding viscous corrections are shown in Table 1 with $2a/d$=0.33 as an example. The studies of Tom (2013) and Son et al. (2016), etc. for vertical axisymmetric floaters with different bottom shapes have proven that the added mass and damping characteristics were similar for heave mode (the only difference is the magnitude). This means the added mass and damping of a floater with a non-FB bottom shape can be estimated by those of a FB floater (which has the same diameter and displacement) with a linear factor correction. For the

convenience of comparison, μ_{33} and λ_{33} of the FB cylindrical floater is used to nondimensionalize $\bar{f}_{\mu,vis}$ and $\bar{f}_{\lambda,vis}$ for all floaters with different bottom shapes. Therefore, $\bar{f}_{\mu,vis}$ and $\bar{f}_{\lambda,vis}$ for non-FB cylindrical floaters not only contain the viscous effect information but also have the information of the geometry difference (different bottom shapes).

Zhang et al. (2016) studied the performance of heaving PA-WECs with different bottom-shape floaters by potential semi-analytical method without any viscous effect being considered. He concluded that the FB cylindrical floater had the largest motion and power response. However, clearly, the sequence is FB > RB > CB > BWB-H > BW in terms of viscous damping. Again, this reveals that the neglection of viscous effect can lead to big errors or even wrong results when studying the performance of heave PA-WECs. The declinations of the viscous damping are 42.7% (RB), 64.4% (CB), and 71.2% (BWB), respectively compared with that of the FB. The reasons are discussed as follows.

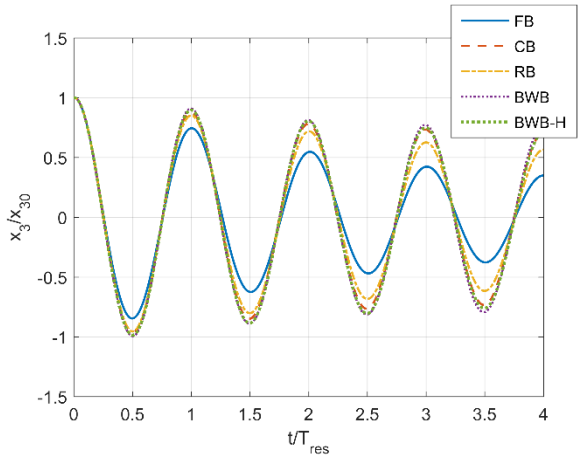

Fig.8. The normalized free-decay curves for cylindrical floaters with different bottom shapes with $2a/d$=0.33.

Table 1 Viscous corrections of cylindrical floaters with different bottom shapes with $2a/d$=0.33.

	FB	RB	CB	BWB	BWB-H
$\bar{f}_{\mu,vis}$	1.56	0.54	0.43	0.47	0.47
$\bar{f}_{\lambda,vis}$	22.47	12.88	8.00	6.47	7.86

The velocity fields are shown in Fig.9 at $t\approx0.25T_{res}$ when the vertical velocity $\dot{x}_3$ of a free-decaying floater reaches the maximum. The variations of the velocity fields of other three around the bottoms are relatively smooth compared with that of the FB. Due to the elimination of the bluff bottom edges, the sudden change of the velocity at the corner disappears, as shown in Fig.9 (a). Relatively, the BWB with the needlelike tip has the smoothest velocity field with the smallest velocity values because of the smoothest streamlined curvature.

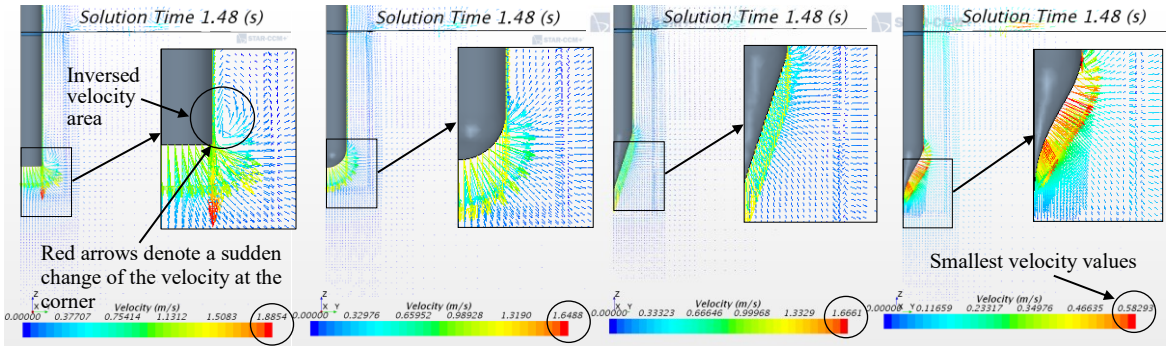

(a) FB (b) RB (c) CB (d) BWB

Fig.9. The velocity fields of the cylindrical floaters with different bottom shapes when $t\approx0.25T_{res}$ with $2a/d$=0.33.

Fig.10 demonstrates the distributions of the wall shear stress on the surfaces of these floaters. The maximum wall shear stress appears at $t\approx0.25T_{res}$ when the vertical velocity of a free-decaying floater reaches the maximum. Due to the inverse velocity area derived from the eddy (Fig.9(a)), there is a region on the surface of the FB floater that has small or even zero shear stress (Fig.10 (a)). Overall, the shear stress of the FB is relatively small compared with the other three. Therefore, the large viscous damping of the FB demonstrated in Fig.8 and Table 1 is mainly contributed by the vortex shedding. For the RB, CB, and BWB, there are no obvious large eddies around the bottom, which means the disturbances to the flow field are weaker. As shown in Table 1, the viscous damping and added mass are smaller than those of FB. For the RB and CB, the areas where connect the convex bottoms have the largest wall stress due to the geometry change. Besides, for the BWB, the wall stress all along the submerged surface of the floater is very smooth because of the four-order streamline shape. Consequently, the BWB has the smallest viscous damping as illustrated in Table 1.

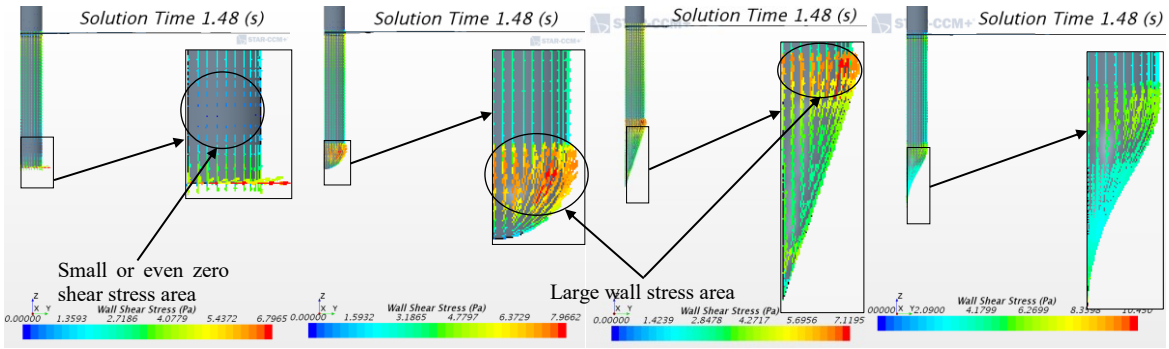

(a) FB (b) RB (c) CB (d) BWB

Fig.10. The wall shear stress on the surface of the cylindrical floaters with different bottom shapes when $t\approx0.25T_{res}$ with $2a/d$=0.33.

As the studies shown above, the BWB has the smallest viscous damping. However, the elimination of the needlelike tip brings 21.5% increase of the viscous damping, while changing very little to the added mass, as demonstrated in Table 1. This reveals that the performance of the small viscous effect of the BWB is highly depended on the sharp needlelike tip which is not practical. Moreover, the difference between

the CB and BWB-H in terms of viscous damping is only 1.8%. Thus, considering of easy manufacturing, floaters with CB are recommended for PA-WECs.

To further study the performance of cylindrical floaters with the CB, the influence of its taper angle coefficient (TAC) on the viscous effect is investigated. The profiles of the CB floaters with different TAC are shown in Fig.11 and the corresponding $\bar{f}_{\mu,vis}$ and $\bar{f}_{\lambda,vis}$ are illustrated in Fig.12. A larger TAC represents a sharper CB and the viscous effect is smaller. With the increasing of the TAC, $\bar{f}_{\mu,vis}$ and $\bar{f}_{\lambda,vis}$ decrease quickly at beginning, then slowly and finally trend to be constant. Therefore, TAC=3.0 is favorable.

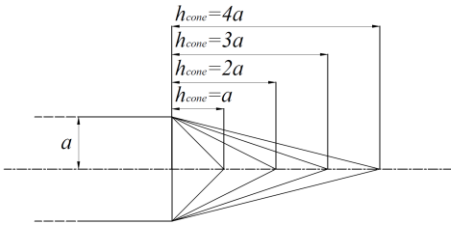

Fig.11. Profiles of cones with different TAC.

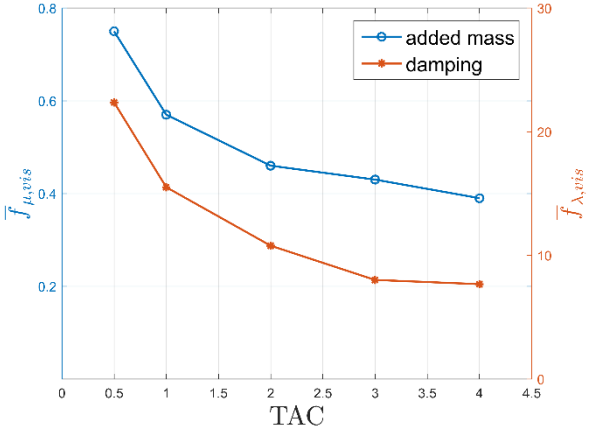

Fig.12. Viscous corrections for CB floaters with different TAC when $2a/d$=0.33.

From Eq. (9), with TAC=3.0 (i.e. $V_{bottom}=\pi a^2 h_{cone}/3=\pi a^3$) and $V=\pi a^2 d$, the expression of d_{cylin} for CB floaters can be derived as

$$d_{cylin} = d - a \tag{10}$$

For a fat floater (i.e. with relatively large $2a/d$), d_{cylin} is small or even not exist when $a>d$. The cone part of the floater may be out of water during the heave motion in waves. Then the nonlinearity of the hydrostatic restoring force is relatively large, which is out of the scope of this paper. Many experiments (Tom, 2013; Son et al., 2016; Madhi et al., 2014) have proven that the results of the experiment and the

linear theory matched very well, when the motion of the floater in waves is under 0.4~0.5d. Therefore, the TAC is set to fulfill the relationship Eq.(11) to ensure that $d_{cylin} \geqslant 0.4d$ for floaters with different $2a/d$. To emphasize, during the real operation of a PA-WEC, the floater may have heave motion that is larger than 0.4d in strongly nonlinear waves. That phenomenon requires a non-linear wave-body interaction theory, which is not discussed in the present paper. For the discussion of the viscous effect of CB floaters in Section 4, the TAC is chosen by the Eq.(11) for floaters with different $2a/d$.

$$\mathrm{TAC}=\begin{cases} 3.0 & 2a/d \le 1.2 \\ \dfrac{3.6}{2a/d} & 2a/d > 1.2 \end{cases} \tag{11}$$

4. Viscous correction and application

This section establishes a viscous correction formula for the CB and FB floaters with $2a/d$ as the independent variable. $\bar{f}_{\mu,vis}$ and $\bar{f}_{\lambda,vis}$ curves of FB and CB floaters are shown in Fig.5 and Fig.13, respectively. The viscous added mass is found to be less than 1.0 for the CB floaters, which is due to the shape effect of the CB. As illustrated in Fig.9, the ability of flow-field-disturbance of the CB floater is smaller than that of the FB. The increase of $\bar{f}_{\mu,vis}$ of CB floaters as shown in Fig.13 (a) is due to the decreasing TAC when $2a/d$>1.2. $\bar{f}_{\lambda,vis}$ of CB floaters are significantly smaller than that of the FB. Taking $2a/d$=0.8, 1.0, and 1.25 as examples, the declination of $\bar{f}_{\lambda,vis}$ of CB floaters compared with that of FB floaters are 70.6%, 66.9%, and 59.8%, respectively.

After many tries, for the viscous correction of both added mass and damping, the function for the curve fitting is chosen as a combination of the exponential and rational functions as illustrated in Eq.(12). The example of curve fitting results of the CB floaters is shown in Fig.13.

$$\bar{f}_{vis} = \frac{\alpha e^{\beta x}}{x^{\sigma} + \delta} \qquad (0.2 < x < 5.0) \tag{12}$$

where $\alpha, \beta, \sigma, \delta$ are the coefficients. For the CB and FB floaters, these coefficients can be found in Table 2. x denotes the independent variable $2a/d$. For this formula, the scope of application is $0.2<x<5.0$, which covers the most possible fatness of floaters for PA-WECs.

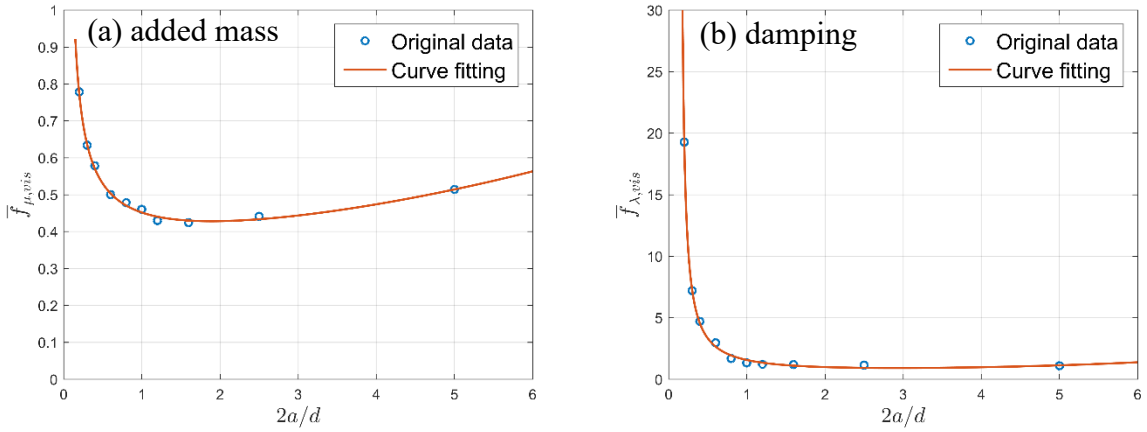

Fig.13. Curve fittings for viscous corrections of CB floaters for different $2a/d$.

Table 2 Parameters of the correction formula for the added mass and damping of the FB and CB cylindrical floaters

		α	β	σ	δ
FB	$\bar{f}_{\mu,vis}$	−3.98100	−0.0009192	−0.41800	−4.28800
	$\bar{f}_{\lambda,vis}$	2.88000	0.29070	1.45400	−0.03169
CB	$\bar{f}_{\mu,vis}$	−0.05625	0.12390	−0.04000	−1.14100
	$\bar{f}_{\lambda,vis}$	0.92960	0.41660	1.18400	−0.09627

The geometry parametric study of a general single-body PA-WEC is taken as an example for the application of the viscous correction formula. The schematic of a general single-body PA-WEC is shown in Fig.14 and the power take-off (PTO) can be taken on the sea bed (e.g. Ulvgård， 2017) or on a fixed structure above water (e.g. Tom, 2013). The optimal damping of a general single-body PA-WEC in regular and irregular waves had been well studied by many literatures, such as Tom (2013), Son et al. (2016), Ulvgård (2017), and Wang et al. (2016), etc. In irregular waves, the optimal damping can be achieved by simple one-variable searching algorithms (Brent, 2013). We adopt the MATLAB one-variable searching function “fminibnd” which is a combination of the golden section search and parabolic interpolation algorithms.

The annual capture width ratio $\bar{C}_{w,year}$ of a PA-WEC can be define as

$$\bar{C}_{w,year} = \frac{P_{m,year}}{2a \cdot P_{w,year}} \tag{13}$$

where $P_{m,year}$ is the annual averaged power. $P_{w,year}$ is the annual averaged wave-power transportation rate per unit wave crest width for a given sea area. $P_{m,year}$ and $P_{w,year}$ can be calculated by adopting the methodology in the paper of Babarit et al. (2012). $\bar{C}_{w,year}$ for CB and FB floaters with different geometries are calculated for the seas around Zhejiang, China (Wu et al., 2015) as an example. The results are shown in Fig.16 and the corresponding long-term sea states (a joint distribution of significant wave height H_s and the wave energy period T_e) are shown in Fig.15. The viscous correction formula is obtained based on the

assumption of small wave amplitude and small motion amplitude. Therefore, only the normal operational sea states are in the research scope of the present paper. Any sea states with Hs larger than 5.0m, which may cause large non-linearity (e.g., green water, wave breaking, etc.), are not considered.

Ignoring the viscous effect can lead to an overestimation of wave energy absorption ability. For FB PA-WECs with and without viscous effect being considered (denoted by "FB-no-vis" and "FB-vis", respectively), the results of $\bar{C}_{w,year}$ are shown in Fig.16 (a) and (b). The maximum $\bar{C}_{w,year}$ of the FB-no-vis is 0.33 and the corresponding diameter and draft of a floater are $2a$=18.5m and d=6.0m. The maximum $\bar{C}_{w,year}$ of the FB-vis is 0.28 which has a 15.2% declination relative to that of the FB-no-vis. Moreover, to achieve the maximum $\bar{C}_{w,year}$, the diameter and draft of a FB-vis floater are found to be $2a$=27.5m and d=5.5m, in which the draft is similar to that of the FB-no-vis (d=6.0m) but the diameter is 48.6% larger than that of the FB-no-vis.

For FB and CB PA-WECs with viscous effect being considered (corresponding to "FB-vis" and "CB-vis", respectively), the results of $\bar{C}_{w,year}$ are shown in Fig.16 (b) and (c). Due to the low viscous effect geometry, the maximum $\bar{C}_{w,year}$ of the CB-vis is 35.7% larger than that of the FB-vis with a smaller CB floater, $2a$=16.5m and d=6.0m, which means more cost-effective. Even compared with the FB-no-vis, the CB-vis still has 15.2% increase of $\bar{C}_{w,year}$ with a smaller floater. Therefore, the CB cylindrical floater has better wave energy absorption ability and is more cost-effective.

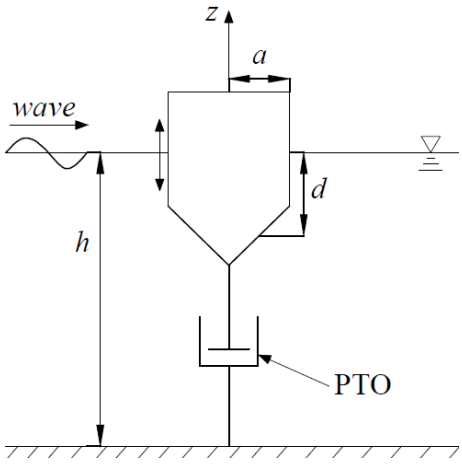

Fig.14. The schematic of a general single-body PA-WEC

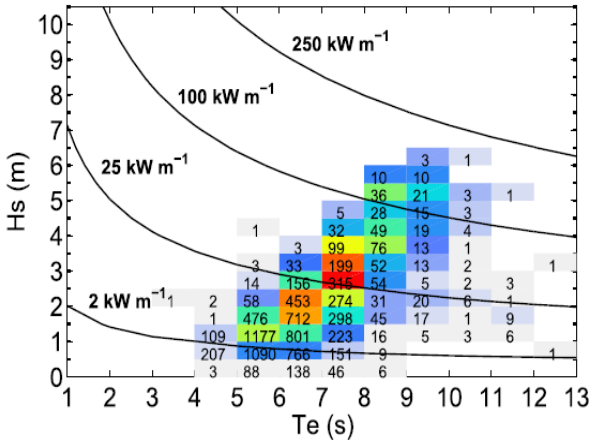

Fig.15. Long-term sea state of the sea area around Zhejiang province, China (Wu et al., 2015).

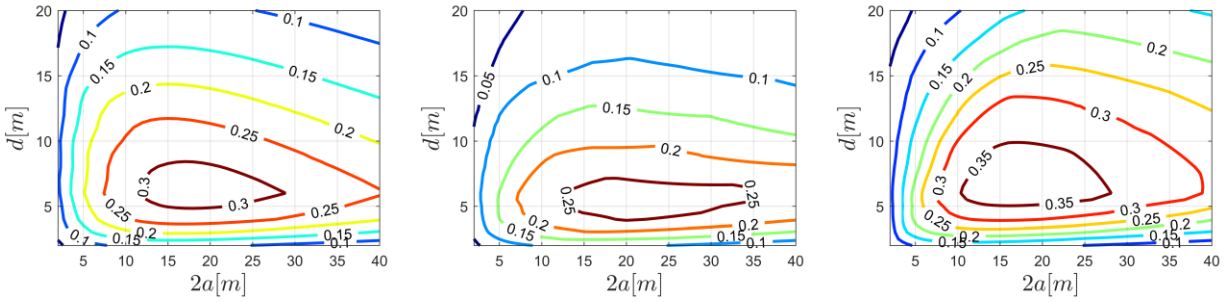

(a) FB-no-vis (b) FB-vis (c) CB-vis

Fig.16. The annual average capture width ratio for CB and FB floaters with different geometries

Table 3 The optimal annual average capture width ratio and corresponding geometry parameters

	FB-no-vis.	FB-vis.	CB-vis.
$\overline{C}_{w,year}$	0.33	0.28	0.38
$2a$ [m]	18.5	27.5	16.5
d [m]	6.0	5.5	6.0

5. Conclusion

The viscous effect of three-dimensional PA-WECs with cylindrical floaters working in heave mode is studied through the free-decay curves of body motion by use of CFD software Star CCM+. Through a comprehensive research, the conclusions are obtained as follows:

(1) The diameter to draft ratio $2a/d$ has a significant influence on the viscous effect of the floater. A fatter floater (with large $2a/d$) has less viscous effect and for very fat floaters, the viscous effect can be neglected.

(2) Considering low viscous effect and easy manufacturing, floaters with conical bottom (CB) are recommended for PA-WECs. The favorable taper angle coefficient (TAC) is 3.0. The viscous damping of floaters with conical bottom (CB) is smaller than that with flat bottom (FB). The

usage of CB can greatly improve the hydrodynamic performance of PA-WECs.

(3) A viscous correction formula for floaters with both FB and CB is put forward with the diameter to draft ratio $2a/d$ as the independent variable. This formula can help researchers to design the floaters and study the performance of PA-WECs with the consideration of fluid viscosity and a fast speed.

(4) An example application, the geometry parameter study for a general PA-WEC, is presented at last. Because of the low viscous effect of CB floaters, the maximum annual capture width ratio $\bar{C}_{w,year}$ of a PA-WEC with the CB in a given long-term sea state is 35.7% larger than that of FB, and the corresponding size of the floater is smaller, which means more cost-effective.

Reference

Babarit, A., Ahmed, H. B., Clément, A. H., Debusschere, V., Duclos, G. and Multon, B., 2006. Simulation of electricity supply of an atlantic island by offshore wind turbines and wave energy converters associated with a medium scale local energy storage. *Renewable Energy*, 31(2), 153-160.

Babarit, A., Hals, J., Muliawan, M. J., Kurniawan, A., Moan, T. and Krokstad, J., 2012. Numerical benchmarking study of a selection of wave energy converters. *Renewable Energy,* 41, 44-63.

Bhinder, M., Babarit, A., Gentaz, L. and Ferrant, P., 2011. Assessment of viscous damping via 3D-CFD modelling of a floating wave energy device. *In 9th European Wave and Tidal Energy Conference.*

Brent, R. P., 2013. *Algorithms for minimization without derivatives*, Courier Corporation.

Caska, A. J., and Finnigan, T. D., 2008. Hydrodynamic characteristics of a cylindrical bottom-pivoted wave energy absorber. *Ocean Engineering*, 35(1), 6-16.

Chen, L., Zang, J., Hillis, A. J., and Plummer, A. R. 2015. Hydrodynamic Performance of a Flap-type Wave Energy Converter in Viscous Flow. *In the Twenty-fifth International Ocean and Polar Engineering Conference*. International Society of Offshore and Polar Engineers.

Drew, B., Plummer, A. R., and Sahinkaya, M. N. 2009. A review of wave energy converter technology. *Proceedings of the Institution of Mechanical Engineers Part A Journal of Power & Energy*, 223(8), 887-902.

Edwards, K. A. and Mekhiche, M., 2014. Ocean power technologies powerbuoy®: system - level design, development and validation methodology.

Faltinsen, O., 1993, *Sea loads on ships and offshore structures*, Cambridge university press.

Goggins, J. and Finnegan, W., 2014. Shape optimization of floating wave energy converters for a specified wave energy spectrum. *Renewable Energy*, 71(11), 208-220.

Jiang, Y. 2015. Computational modeling of rolling wave-energy converters in a viscous fluid. *Journal of Offshore Mechanics & Arctic Engineering*, 137(6), 1-9.

Jin, S. and Patton, R., 2017. Geometry Influence on Hydrodynamic Response of a Heaving Point Absorber Wave Energy Converter. *European Wave and Tidal Energy Conference*.

Li, Y. and Yu, Y. H., 2012. A synthesis of numerical methods for modeling wave energy converter-point absorbers. *Renewable and Sustainable Energy Reviews*, 16(6), 4352-4364.

Madhi, F., Sinclair, M. E. and Yeung, R. W., 2014. The Berkeley Wedge: an Asymmetrical Energy-Capturing Floating Breakwater of High Performance. *Marine Systems & Ocean Technology, Journal of SOBENA*, 9(1), 05-16.

Mccabe, A. P. and Aggidis, G. A., 2009. Optimum mean power output of a point-absorber wave energy converter in irregular waves. *Proceedings of the Institution of Mechanical Engineers Part A Journal of Power & Energy*, 223(223), 773-781.

Ning, D. Z., Wang, R. Q., Zou, Q. P., and Teng, B. 2016. An experimental investigation of hydrodynamics of a fixed OWC wave energy converter. *Applied Energy*, 168, 636-648.

Ning, D. Z., Shi, J., Zou, Q. P., and Teng, B. 2015. Investigation of hydrodynamic performance of an OWC (oscillating water column) wave energy device using a fully nonlinear HOBEM (higher-order boundary element method). *Energy*, 83, 177-188.

Palm, J., Eskilsson, C., Paredes, G. M. and Bergdahl, L., 2016. Coupled mooring analysis for floating wave energy converters using cfd: formulation and validation. *International Journal of Marine Energy*, 16, 83-99.

Penesis, I., Manasseh, R., Nader, J. R., De Chowdhury, S., Fleming, A., Macfarlane, G. and Hasan, M. K., 2016. Performance of ocean wave-energy arrays in Australia. *In 3rd Asian Wave and Tidal Energy Conference (AWTEC 2016)*, Vol. 1, pp. 246-253.

Shek, J. K. H., Macpherson, D. E., Mueller, M. A. and Xiang, J., 2009. Reaction force control of a linear electrical generator for direct drive wave energy conversion. *Renewable Power Generation Iet*, 1(1), 17-24.

Son, D., Belissen, V. and Yeung, R. W., 2016. Performance validation and optimization of a dual coaxial-cylinder ocean-wave energy extractor. *Renewable Energy*, 92, 192-201.

Tom, N. M., 2013. *Design and control of a floating wave-energy converter utilizing a permanent magnet linear generator.* PhD Thesis, University of California, Berkeley.

Ulvgård, L., 2017. *Wave Energy Converters: An experimental approach to onshore testing, deployments and offshore monitoring,* PhD Thesis, Acta Universitatis Upsaliensis.

Vantorre, M., Banasiak, R. and Verhoeven, R., 2004. Modelling of hydraulic performance and wave energy extraction by a point absorber in heave. *Applied Ocean Research*, 26(1), 61-72.

Wang, L., Son, D. and Yeung, R. W., 2016. Effect of mooring-line stiffness on the performance of a dual coaxial-cylinder Wave-Energy Converter. *Applied Ocean Research*, 59, 577-588.

Weber, J., Mouwen, F., Parish, A. and Robertson, D, 2009. Wavebob—research & development network and tools in the context of systems engineering. I*n Proc. Eighth European Wave and Tidal Energy Conference*, Uppsala, Sweden.

Wu, S., Liu, C. and Chen, X., 2015. Offshore wave energy resource assessment in the east china sea. *Renewable Energy*, 76, 628-636.

Yeung, R. W. and Jiang, Y., 2011. Effects of shaping on viscous damping and motion of heaving cylinders. *Journal of Offshore Mechanics & Arctic Engineering*, 136(4), 825-836.

Zhang, W. C., Liu, H. X., Zhang, L. and Zhang, X. W., 2016. Hydrodynamic analysis and shape optimization for vertical axisymmetric wave energy converters. *China Ocean Engineering,* 30(6), 954-966.